Engineering 7 (2021) 1557–1565

Contents lists available at ScienceDirect

Engineering

journal homepage: www.elsevier.com/locate/eng

Research
Immunology—Article

High-Affinity Decoy PD-1 Mutant Screened from an Epitope-Specific Cell Library

Hao Liu [a,b,#], Chunxia Qiao [a,#], Naijing Hu [a,c,#], Zhihong Wang [a,d], Jing Wang [a], Jiannan Feng [a], Beifen Shen [a], Yuanfang Ma [b,*], Longlong Luo [a,*]

[a] State Key Laboratory of Toxicology and Medical Countermeasures, Beijing Institute of Pharmacology and Toxicology, Beijing 100850, China
[b] Joint National Laboratory for Antibody Drug Engineering, The First Affiliated Hospital, School of Medicine, Henan University, Kaifeng 475004, China
[c] School of Life Science and Biopharmaceutics, Shenyang Pharmaceutical University, Shenyang 110016, China
[d] School of Basic Medicine and Clinical Pharmacy, China Pharmaceutical University, Nanjing 210009, China

ARTICLE INFO

Article history:
Received 17 October 2019
Revised 17 August 2020
Accepted 16 November 2020
Available online 13 July 2021

Keywords:
Decoy PD-1
PD-L1
Mammalian cell library
Epitope-oriented

ABSTRACT

Immunotherapy with anti-programmed cell death protein-1 (PD-1)/programmed cell death ligand-1 (PD-L1) monoclonal antibodies has become routine in the treatment of many kinds of human cancers, such as lung cancer, intestinal cancer, and melanoma. The PD-1/PD-L1 pathway inhibits T cell activation in the micro-environment, making it an attractive target against cancer. Wild-type (WT) PD-1 ectodomain has been shown to have difficulty blocking PD-1/PD-L1 mixture formation due to its low affinity. The present work uses three-dimensional (3D) crystal complex structures to analyze the interaction by which PD-1 binds to PD-L1 or PD-L2. It also reports on a theoretical study of the binding mode between PD-1 and its clinical antibody Opdivo. Based on the theoretical binding analysis of PD-1 and its ligands (i.e., PD-L1 and PD-L2) or antibody (Opdivo), a small-content, epitope-oriented mammalian cell library was established for PD-1. After three rounds of cell sorting, the decoy PD-1 mutant 463, which presented a higher affinity than WT PD-1 to the PD-L1 (the affinity has increased by almost three orders of magnitude) was screened out. It exhibited an inhibitory effect against PD-1 to prevent it from forming mixtures with PD-L1, which was similar to the effect of the commercial anti-PD-L1 antibody atezolizumab (ATE). The median effective concentration (EC_{50}) value of the decoy mutant was 0.031 $\mu g \cdot mL^{-1}$ in comparison with 0.063 $\mu g \cdot mL^{-1}$ for ATE; both values were much lower than that of WT PD-1, at 2.571 $\mu g \cdot mL^{-1}$. The 463 decoy mutant reversed the inhibitory function of PD-1 in T cell activation; furthermore, 10 $mg \cdot kg^{-1}$ of 463 inhibited about 75% of tumor growth *in vivo* in a MC38 transgenic xenograft mice model, which was similar to the activity of ATE. More interestingly, an even lower dose of 463 (2 $mg \cdot kg^{-1}$) showed a better effect than 10 $mg \cdot kg^{-1}$ of WT PD-1. This work offers the decoy 463 with an improved curative effect, which holds potential to become a good option against PD-1/PD-L1-related cancers.

1. Introduction

Lymphocyte activity is normally regulated by inhibitory, stimulatory, and co-stimulatory cues. In T lymphocytes, the balance between negative and positive signals shapes T cell response on exposure to reactive peptides or the major histocompatibility complex (MHC) [1]. Cancer "antigens" are recognized by the T cell receptors (TCRs) on cytotoxic T lymphocytes and, in many cases, prompt an endogenous response against cancer by the immune system [2]. However, cancer cells sometimes benefit from immunosuppressive signals in order to escape immune surveillance [3]. For example, the signal pathway of the immune checkpoint programmed cell death protein-1 (PD-1) and one of its ligands, programmed cell death ligand-1 (PD-L1), presents a barrier to immune function by blocking T cell activation [4]. PD-1/PD-L2 and PD-L1/cluster of differentiation 80 (CD80) also trigger inhibitory signals in T cells. Normally, the PD-1/PD-L1 pathway prevents excessive T cell activation and maintains immune tolerance to self-antigens [5]. However, in various cancers, such as lymphoma, melanoma, lung cancer, and breast cancer, PD-L1

* Corresponding authors.
E-mail addresses: luolong_long@126.com (L. Luo), mayf@henu.edu.cn (Y. Ma).
# These authors contributed equally to this work.

https://doi.org/10.1016/j.eng.2020.11.011

is often over-expressed and prevents the anti-tumor effect of T lymphocytes by binding to PD-1 on the T cell surface in the tumor microenvironment of the cancer [6–10]. PD-1 initiates the inhibitory signal cascade by means of its intracellular domain, which contains a switch motif to activate tyrosine phosphatases SHP that oppose TCR signaling and an immunoreceptor tyrosine-based inhibitory motif [11]. PD-1/PD-L1 inhibits T proliferation, cytokine release, and cytotoxicity, thus resulting in exhaustion and/or apoptosis of T lymphocytes in cancer [12]. Consequently, the PD-1/PD-L1 pathway has been identified as a key molecule for cancer immunotherapy, and several anti-PD1/PD-L1 antibody drugs have been approved to enter the market, such as Keytruda/pembrolizumab, Opdivo/nivolumab, and Tecentriq/atezolizumab (ATE). These drugs have demonstrated impressive therapeutic function across abroad set of cancer subtypes in both advanced and metastatic stages [13–17]. In clinics, a large number of cancer patients have demonstrated long-term responses to anti-PD-1/PD-L1 immunotherapy [14]. The results were impressive enough to accelerate the approval of pembrolizumab and nivolumab in 2014[†] [18,19]. Recently, evidence has shown that the anti-PD-1 antibodies are more effective than traditional chemotherapy in metastatic melanoma treatment [20–22]. Nivolumab has also shown satisfactory clinical results in patients with metastatic squamous non-small cell lung cancer (NSCLC). It has been approved as the first monotherapy drug in more than 15 years to demonstrate proven superior overall survival[‡] (OS) compared with the standard strategy. Antibodies block PD-1/PD-L1 signaling, reverse the immunosuppressive status in tumors, and activate T lymphocytes to suboptimal efficacy; in addition, traditional antibodies show their ability by means of cytotoxic immune responses through natural killer (NK) cells or macrophages (e.g., antibody-dependent cell-mediated cytotoxicity (ADCC) or antibody-dependent cell-mediated phagocytosis (ADCP)) [23]. Besides, anti-PD-1 antibodies block PD-1 from binding to its ligands (PD-L1 or PD-L2), while anti-PD-L1 antibodies block the PD-1/PD-L1 or PD-L1/CD80 signal pathways [24,25]. Similar to the monoclonal antibodies used in most studies when blocking the PD-1/PD-L1 pathway, the extracellular domain of PD-1 can be administered as a competitive antagonist. The PD-1 ectodomain is smaller than the monoclonal antibody (whose molecular weight is about 150 kDa), with a molecular weight of about 30 kDa, so it can more easily enter the cancerous region. However, wild-type (WT) PD-1 binds to PD-L1 with a low affinity ($\sim 10^{-6}$ mol·L^{-1}) [26]; therefore, it is difficult for WT PD-1 to block the inhibitory signal of PD-1/PD-L1. Previously, we tried to establish an epitope-targeted mammalian cell-displayed library, and obtained a novel anti-human PD-1 antibody [27]. We thus considered whether a PD-1 mutant by *in vitro* affinity evolution could exhibit satisfactory anti-tumor responses like antibodies. Thus, based on the key residues of PD-1 that bind to PD-L1, we established an epitope-specific cell-surface display library that contained millions of PD-1 mutants, from which higher affinity PD-1 mutants were screened out in order to obtain a mutant with better function than WT PD-1.

2. Materials and methods

2.1. Reagents

Human PD-1, PD-L1, and CD80 and human/murine PD-L2 were purchased from SinoBiological (Cat. Nos: 10377-H02H, 10084-H02H, and 10698-H02H). Allophycocyanin (APC) conjugation (e.g., PD-1) and biotin conjugation (e.g., PD-1, PD-L1, and PD-L2) were prepared by Jiaxuan Biotech Co., Ltd. (China). The interferon (IFN)-γ detection kit was purchased from BioLegend, Inc. (USA), and the anti-PD1 antibody Opdivo and the anti-PD-L1 antibody ATE were prepared in our lab according to the patented DNA sequence. MIL50 was an anti-ricin monoclonal antibody prepared in our lab. Streptavidin–horseradish peroxidase (HRP), streptavidin–APC, isotype control human immunoglobulin G (IgG) (Cat. No: 02-7102), and goat anti-human IgG (H + L) secondary antibody (HRP-conjugated; Cat. No: #A18805) were from Invitrogen (USA). Dulbecco's modified Eagle medium (DMEM; Cat. No: 11965-092), DMEM-F12 media (Cat. No: C11330500BT), and fetal bovine serum (FBS; Cat. No: 10438-034) were from Thermo Fisher (USA). ExpiCHO expression system were from Thermo Fisher (Cat. No: A29133). The mammalian cell library plasmids with membrane display, pFRT-FTMK, and the vector to bear the full Igs, pFRT-IgG1K, were constructed in our lab [27]. The above two vectors are derived from Invitrogene's commercial pcDNA5/FRT vector (Cat. No: V601020), which can be used in conjunction with the Flp-In™ system. This vector contains flippase (Flp)-recombination target (FRT) characteristic sequence. A recombinant enzyme, Flp, can cut and insert the plasmid into the genome at specific sites with the same characteristic sequence. All other reagents were obtained from a commercial source at analytical grade.

2.2. Cell culture

Chinese hamster ovary (CHO)-K1–PD-L1 cells were prepared by transfecting PD-L1 genes to CHO-K1 cells (American Type Culture Collection (ATCC), USA). Human embryonic kidney epithelial cells 293T (ATCC, USA) and MC38 (mouse PD-L1 knock-out, human PD-L1 knock-in) were obtained from the Shanghai Model Organisms Center, Inc. (China); the CHO-Flp-In™ cells were cultivated in DMEM/F12 medium supplemented with 100 units·mL^{-1} of penicillin, 100 units·mL^{-1} of streptomycin, 100 μg·mL^{-1} of zeocin, and 10% heat-inactivated FBS. The 293T cells were cultured in DMEM supplemented with 10% heat-inactivated FBS, 100 units·mL^{-1} penicillin, and 100 units·mL^{-1} streptomycin. Cells were cultured in a humidified incubator (Thermo Fisher) at 37 °C in 5% carbon dioxide (CO_2).

2.3. Computer-aided design of the PD-1 library

Atheoretical three-dimensional (3D) structure of human PD-1 that binds to PD-L1 was constructed using InsightII (version 2005; Molecular Simulations, USA) and optimized using the modules Discover and Discover_3. The non-bonded cutoff was 10 Å (1 Å = 0.1 nm), and atomic charges and non-bonded parameters were taken as defaults. A distance-dependent dielectric constant was used for *in vacuo* calculations. The model was minimized using the steepest descent (2000 steps) and conjugate gradient (5000 steps) methods, respectively. According to the theoretical structure of the PD-1 and PD-L1 complex, the potential amino acid positions where PD-1/PD-L1 recognize each other are predicted. In order to prove the correctness of the theoretical prediction, the key amino acid of PD-L1 involved in the recognition of PD-1 was replaced with alanine to verify that the key site of the role of PD-L1 and PD-1. In the case that the verification model is correct, we designed a series of PD-1 mutations. We replaced the PD-L1-contacting sites of PD-1 with residues that had a similar carbon chain backbone to PD-1 but longer side-chains, which bound to PD-L1 more tightly. To ensure the theoretical library quality, the 3D complex structures of PD-1 and PD-L2, PD-1 and its clinical antibody Opdivo were also studied using the same theoretical method.

[†] http://www.fda.gov/NewsEvents/Newsroom/PressAnnouncements/ucm436534.htm.

[‡] http://www.fda.gov/Drugs/InformationOnDrugs/ApprovedDrugs/ucm436566.htm.

2.4. Flow cytometry

The experiments were performed on ice. Cells (5×10^5) were washed, suspended in assay buffer (phosphate-buffered saline (PBS) containing 2% FBS), and then incubated with proteins (e.g., PD-L1–biotin) or antibody on ice for 30 min. If necessary, after washing, the cells were incubated with APC-conjugated streptavidin determined using a BD FACSCalibur™ (USA). The cell fluorescence density was collected and analyzed with BD CellQuest Pro software.

2.5. Design and construction of the PD-1 library

Based on the computer-aided design results, five mutants (M1–M5) on PD-1, which may be the key site for PD-L1 binding, were first synthesized by means of the alanine replacement method and were displayed on the 293T cell surface by cell transfection. The specific amino acid substitutions on PD-1 and free energy result of binding to PD-L1 before and after mutation are shown in Table 1. Fluorescence activated cell sorting (FACS) data testing on the PD-1 mutants binding to PD-L1 was used to identify the importance of the mutated regions, and 13 key sites of PD-1 were selected and replaced with 1–3 kinds of amino acids (Table 2) that held potential to enhance the affinity of PD-1 to bind to PD-L1. This resulted in a small-content, PD-1-targeting library. Using overlapping polymerase chain reaction (PCR), we synthesized the library genes, subcloned them to pFRT-FTMK, and transfected them into CHO-Flp-In™ cells.

Table 1
The specific amino acid substitutions to alanine on PD-1 that may interact with PD-L1 and the calculation of the interaction energy based on the computer-aided design.

PD-1 mutant	Key residues in PD-1 interact with PD-L1	Interaction energy between PD-1 and PD-L1 before PD-1 mutant (kJ)	Interaction energy between PD-1 and PD-L1 after Ala replacement in PD-1 (kJ)
PD-1 M1	$Asn^{66}Tyr^{68}$	−218.96	−108.29
PD-1 M2	$Asn^{74}Gln^{75}Thr^{76}Asp^{77}Lys^{78}$	−218.96	−98.31
PD-1 M3	$Tyr^{45}Glu^{46}Asp^{48}Asn^{49}$	−218.96	−215.38
PD-1 M4	$Ile^{126}Leu^{128}Lys^{131}Ile^{134}Glu^{136}$	−218.96	−94.29
PD-1 M5	$Glu^{84}Asp^{85}Arg^{86}Ser^{87}Gln^{88}$	−218.96	−106.83

Asn: asparagine; Tyr: tyrosine; Gln: glutamine; Thr: threonine; Asp: aspartic acid; Lys: lysine; Glu: glutamic acid; Ile: isoleucine; Leu: leucine; Arg: arginine; Ser: serine.

Table 2
Design of high affinity PD-1 mutations to form a small-content cell library.

Key amino acid	Alternative amino acid replacement (free energy ≤ −119 kJ)	Merger codon
Val^{64}	His, Ile, Leu	AWS
Arg^{69}	Glu	RRS
Asn^{74}	Gly, Ser	RRC
Ala^{81}	Val, Leu, Ile	VYC
Glu^{84}	Gln, Asp	SAS
Arg^{86}	His, Tyr	YRC
Ser^{87}	Asn	ARC
Gly^{90}	Ala, Val, Leu	SBC
Gln^{91}	Tyr, Phe	YWS
Leu^{122}	Ile, Gln	MWS
Ser^{127}	Tyr, Phe	THC
Ala^{129}	Gly	GSC
Ala^{132}	Val, Leu, Ile	BYC

M = A/C, R = A/G, W = A/T, S = G/C, Y = C/T, V = A/G/C, H = A/C/T, and B = G/C/T represents the merger of several bases. In theory, the frequency of each base in the synthesis process is equal.
Val: valine; Ala: alanine; Gly: glycine; Phe: phenylalanine; His: histidine.

2.6. FACS sorting

A total of 5×10^7 cells screened out from the cell libraries were collected and re-suspended in 1 mL of PBS supplemented with 2% FBS. The cells were then stained with 2 $\mu g \cdot mL^{-1}$ PD-L1–biotin, after incubating at 4 °C for 30 min, APC-conjugated streptavidin was added and incubate under the same conditions. WT PD-1 cells were set as the control. The fluorescence data was analyzed, and the cells with stronger binding capacity were sorted using the FACS Aria III flow cytometer. Selected PD-1 mutant genes from the library were sequenced, subcloned, and expressed using our Flp–FRT mammalian cell system [27].

2.7. Enzyme-linked immunosorbent assay

Enzyme-linked immunosorbent assay (ELISA) plates were coated with 1 $\mu g \cdot mL^{-1}$ protein (e.g., PD-1) at 4 °C overnight and then blocked in PBS supplemented with 1% bovine serum albumin (BSA) containing 0.05% Tween-20 for an hour at 37 °C. Proteins (e.g., PD-L1–biotin) were then added. After washing, horseradish peroxidase conjugated streptavidin was added for 1 h of incubation at room temperature (RT). Binding signals were visualized using tetramethylbenzidine (TMB) substrate (Cat. No: 00–4201-56; Invitrogen), and the absorbance was measured using an ELISA reader at 450 nm.

2.8. Biacore

Surface plasmon resonance experiments were performed at 25 °C using a Biacore T200 machine with HBS-EP as the running buffer (Cat. No: BR-1003–99; GE Healthcare, USA). For these measurements, PD-L1 or PD-L2 was coupled on a CM5 chip at pH 5.0 using an amine coupling kit (Cat. No: BR-1001–88; GE Healthcare). A dilution series of the PD-1 mutants (from 3.125 to 50 $nmol \cdot L^{-1}$) was passed through both flow cells at 30 $\mu L \cdot min^{-1}$ to record the association phase (120 s). The dissociation phase was monitored for 1200 s and was triggered by replacing the sample solution with HBS-EP. Bulk refractive index differences were corrected by subtracting the response obtained on the reference flow cell (the first flow cell). After each cycle, the sensor surface was regenerated via a short treatment with 10 $mmol \cdot L^{-1}$ glycine–HCl (pH 2.1). The binding kinetics were recorded and analyzed with the Biacore T200 evaluation software (GE Healthcare) using the 1:1 binding model. The WT PD-1 was set as the control, and the solvent (sample buffer) was set as the negative control. The background was deducted according to the V-baseline in order to obtain the kinetic curves and calculate the dissociation constant (K_D value).

2.9. Mouse tumor xenograft models

Female, 12- to 14-week-old transgenic mice C57BL/6j (murine PD-1 knock-out and human PD-1 knock-in mice) were purchased from Shanghai Model Organisms Center, Inc. (China) and housed in filter-top cages (five mice per cage) in an specific pathogen-free (SPF)-level facility fed with sterilized food and water. We followed the "*Animal Research: Reporting of* In Vivo *Experiments*" (ARRIVE) guidelines[†] for the use of mice during the study. We observed animal ethics during the research according to the "3R" principles of replacement, reduction, and refinement; the use or treatment of the mice was in strict agreement with the guidelines for the care and use of research animals, and was approved by the Animal Ethics Committee of the Beijing Institute of Pharmacology

[†] https://www.nc3rs.org.uk/arrive-guidelines.

and Toxicology. Before we injected the cancer cells, the mice were checked every day for a week for signs of discomfort and for general appearance. Then, a genetically engineered cell line that replaced the mouse PD-L1 gene *in situ* with a human PD-L1 molecule on the basis of the MC38 cell line, and we abbreviated it as MC38 (hPD-L1). Cultivate the above cells to the logarithmic growth phase and then 1×10^6 MC38 (hPD-L1) cells per mouse were injected intravenously. In about a week, when the tumor volume had reached 80 mm^3, the mice were given an intraperitoneal injection with the anti-PD-L1 antibody ATE, WT PD-1, PD-1 mutant 463, or the isotype control (anti-ricin antibody MIL50). The mice were observed twice a week to measure the mice weight and tumor size for another four weeks. After the assay, the mice were sacrificed using anesthesia with ketamine followed by the cervical dislocation method; we then used deep-freezing to confirm death.

2.10. Statistical analysis

Statistical analysis was performed by Student's *t*-test or by repeated measures of one-way analysis of variance (ANOVA) followed by a Tukey *post hoc* test. *In vivo* differences were analyzed by two-way ANOVA followed by a Bonferroni *post hoc* test. The significance of the dose escalation experiment was tested with a normal linear mixed effect model. Treatments were considered significant when $p < 0.05$.

3. Results

3.1. The epitope of PD-1 to bind to PD-L1 was superimposed

Using homological modeling, docking, and dynamic simulation methods, we modeled the theoretical structures of PD-1 and its ligands PD-L1 or PD-L2, or the anti-PD-1 antibody Opdivo, respectively. Using the 3D complex theoretical structure of PD-1 and PD-L1, the initial affinity-matured library was constructed. To guarantee the theoretical affinity-matured library quality, the binding mode between PD-1 and PD-L2, PD-1 and Opdivo was analyzed theoretically. Using the binding mode and key residues of PD-1 identified by PD-L2 and Opdivo, the affinity-matured library was optimized and the important residues were predicted. As shown in Fig. 1(a), the key amino acid sites for the interaction between

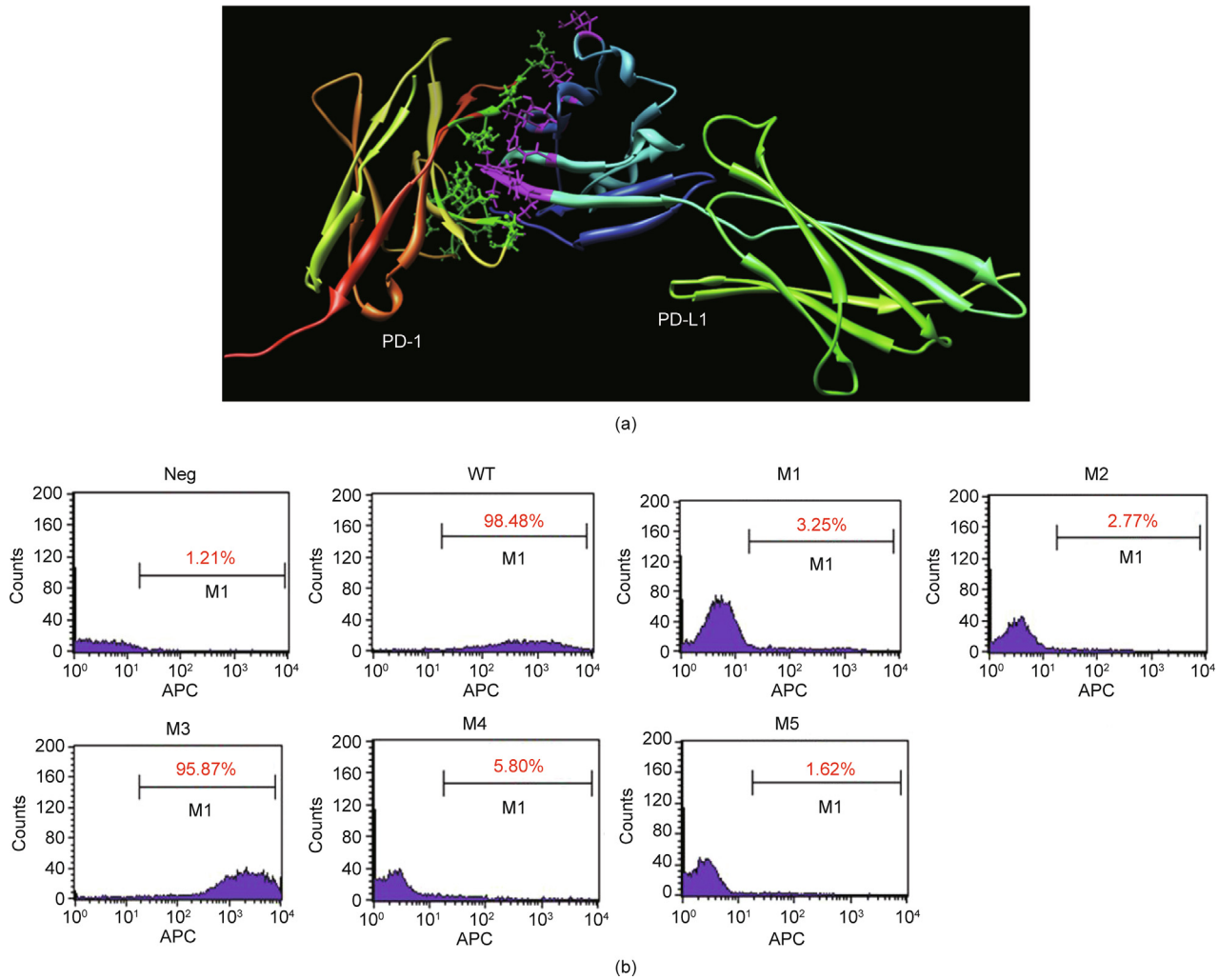

Fig. 1. Epitope identification of PD-1 to bind PD-L1. (a) Theoretical structure of the PD-1 and PD-L1 complex. The green sticks represent key sites in PD-1, while the purple sticks are key sites in PD-L1 that bind with PD-1. The sites (green and purple sticks) positioned in the interface between PD-1 and PD-L1 are the key sites for direct contact. (b) Flow cytometry detection of the sites on PD-L1 that bind to the WT PD-1 or its mutants displayed on the 293T cell surface. The mutants were designed and their DNA sequences were synthesized using the alanine replacement method. The transfected cells were incubated with biotin-conjugated PD-L1 followed by APC-conjugated streptavidin. The M1, M2, M4, and M5 mutants lost their binding capacity, indicating that the mutated residues in these mutants were key sites allowing PD-1 binding to PD-L1. Neg: negative control.

PD-1 and PD-L1 are represented by different colored stick structures.

The PD-1 mutant-expressing cells (M1–M5) were incubated with biotin-conjugated PD-L1 followed by APC-conjugated streptavidin. M1, M2, M4, and M5 were confirmed to be important for PD-1 binding to PD-L1, as they showed significant reduction or complete loss of binding to PD-L1 (Fig. 1(b)). Based on the FACS data shown in Fig. 1(b), the structure of the PD-1/PD-L1 complex was optimized. Residues Val^{64}, Arg^{69}, Asn^{74}, Ala^{81}, Glu^{84}, Arg^{86}, Ser^{87}, Gly^{90}, Gln^{91}, Leu^{122}, Ser^{127}, Ala^{129}, Ala^{132} located on PD-1 were found to be important and to have the potential, if mutated, to improve PD-1's affinity for binding to PD-L1.

3.2. Directed evolution of higher affinity PD-1 mutant with the epitope-specific cell library

WT PD-1 can bind to PD-L1 with low affinity, so it is difficult to block PD-1/PD-L1 interaction in the cancer micro-environment. The higher affinity PD-1 mutants could block PD-1/PD-L1 mixture formation as a potential decoy drug (Fig. 2(a)). Based on the structure information and the key sites of PD-1, we designed the higher affinity mutations of each amino acid. During the design, it was important to keep the epitope of each mutant recognized by PD-L1. That is, the mutated sites needed to have structural, physical, or chemical characteristics similar to those of the WT residues. Therefore, the library was a small-content library to contain only higher affinity PD-1 mutations with a persistent epitope. By means of overlap PCR, the DNA sequences of the PD-1 mutants were amplified. An electrophoresis results showed the transfer bands of DNA library fragments in agarose gel were the same size as the theoretical bands with a molecular weight of about 650 base pairs (bp) (Fig. S1 in Appendix A) and the mutated sequences were inserted into the library vector pFRT-FTMK through conventional molecular biology digestion and connection methods.

To confirm the viability of the library, the plasmids were sequenced using anext-generation sequencing method, and the designed amino acids were analyzed to show their distribution (Fig. S2 in Appendix A). Then, the library plasmids of various PD-1 mutants were transfected to the CHO-Flp-In™ cells and

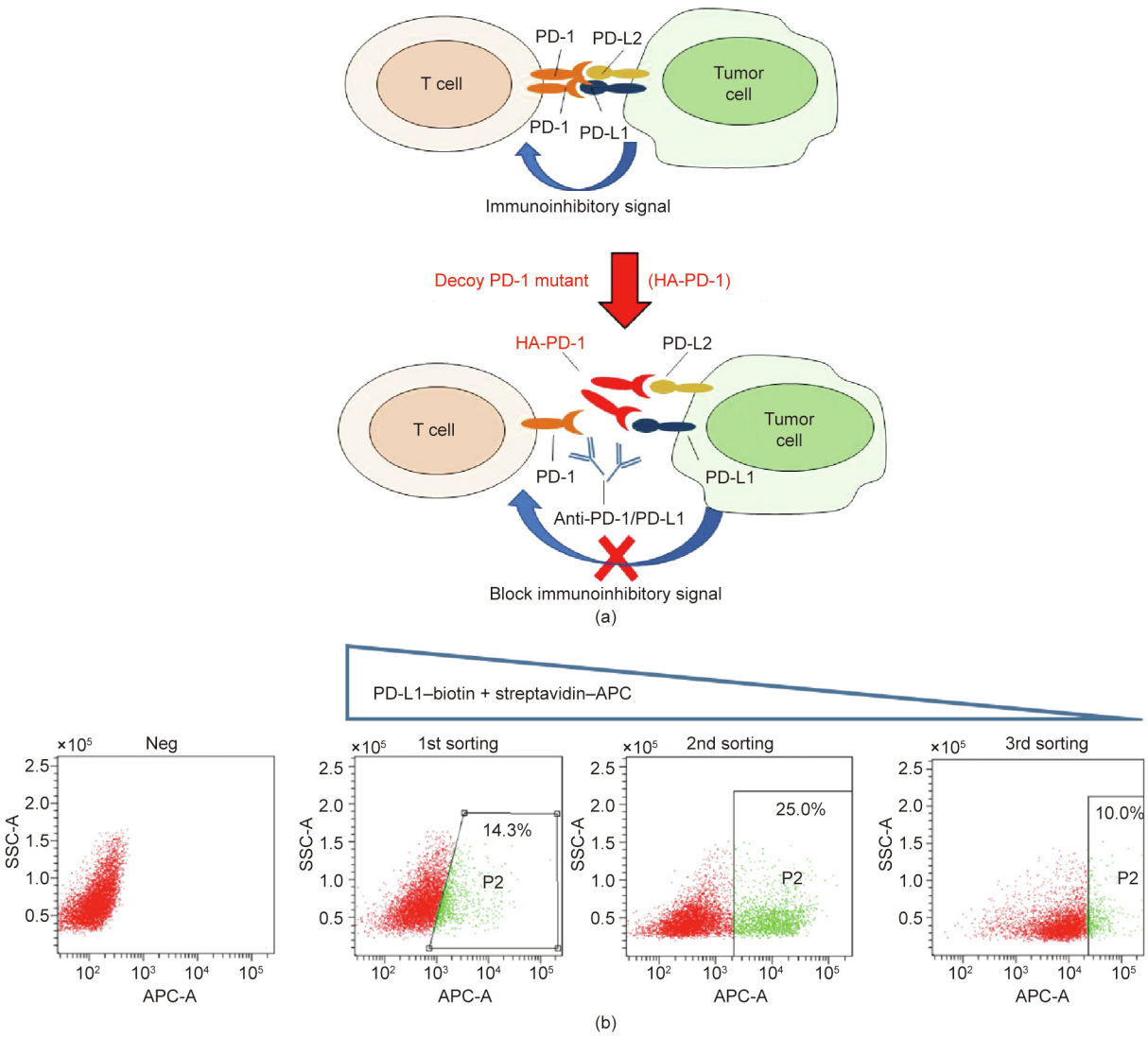

Fig. 2. Directed evolution of high-affinity PD-1 mutants using the cell surface display method. (a) High affinity PD-1 (HA-PD-1) decoy molecule design schematic diagram, the wild type PD-1 molecule cannot effectively block the immunosuppressive signal between PD-1 and PD-L1, improving the affinity between PD-1 and PD-L1 can effectively block the immunosuppressive signal between PD-1 and PD-L1, and release the tumor-killing ability of immune cells. (b) Three rounds of screening of the PD-1 library. After each selection, the cell clones possessed stronger PD-L1 binding capacity. SSC-A: side scatter area; APC-A: allophycocyanin area; HA: high affinity; Neg: negative control.

displayed on the cell surface. High-affinity clones were screened out using three rounds of cell sorting (Fig. 2(b)). After each round of cell sorting, the clones possessed stronger PD-L1 binding capacity. A total of 29 monoclones were selected, and the mutant sequences were sequenced. Then the mutant sequence genes were inserted into the pFRT-IgG1Fc vector to prepare the PD-1 mutants Fc fusion proteins in the 293T cells. The supernatant of the transfected cells was collected, diluted, and incubated with coated PD-L1/PD-L2 to compete with the WT PD-1.

ELISA detection showed the binding capacity of the 29 PD-1 mutants as well as WT PD-1 to bind to PD-L1 or PD-L2 (Fig. S3 in Appendix A). Nine mutants with potentially enhanced binding capacity were chosen for further antagonistic identification: 408, 431, 407, 410, 446, 411, 463, 506, and 576. These mutants could bind to human PD-L1 (Fig. S4 in Appendix A) or human PD-L2 (Fig. S5 in Appendix A) in a dose-dependent manner. Furthermore, they inhibited WT PD-1 from binding to PD-L1 or PD-L2 (Figs. S6(a) and (b) in Appendix A), suggesting a potential use as decoy proteins against the PD-1/PD-L1 signal. Biacore analysis was used to confirm five PD-1 mutants with the highest affinity for binding PD-L1 or PD-L2 (Table 3).

In contrast to the WT PD-1 (1.00×10^{-6}) [26], their affinity constants range from 1.28×10^{-6} to 2.06×10^{-9}, indicating the stronger binding capacity of these mutants. One of the mutants, 463, possessed a much slower dissociation constant (2.06×10^{-3}) than the others. Moreover, the five mutants bound to PD-L2 with affinity constants ranging from 2.67×10^{-8} to 6.95×10^{-9}, which are higher than that of the WT PD-1. According to the flow cytometry data, two PD-1 mutants, 463 and 506, inhibited PD-1 from binding to the surface of PD-L1. They both showed much better inhibitory activity than WT PD-1, and a similar or even better effect than ATE (Fig. S6(c)). We established a stable cell line of the two; however, the expression level of 506 in ExpiCHO expression system was much lower than that of 463, so we chose 463 for further research.

Mutant 463 bound to human PD-L1 in a dose-dependent manner with an EC_{50} value of 0.031 μg·mL^{-1}, which was lower than that of WT PD-1 (2.571 μg·mL^{-1}) and ATE (0.063 μg·mL^{-1}), suggesting the possibility that 463 could reverse PD-1/PD-L1 in future applications (Fig. 3(a)). As shown in Fig. 3(b), 463 bound to human PD-L2 in a dose-dependent manner with an EC_{50} value of 0.63 μg·mL^{-1}, which was much lower than that of WT PD-1 (> 6 μg·mL^{-1}); 463 also bound to murine PD-L1 with an EC_{50} value of 0.97 μg·mL^{-1}, which was much lower than that of WT PD-1 (132.5 μg·mL^{-1}) (Fig. 3(c)).

3.3. PD-1 mutant 463 blocked PD-1/PD-L1 formation to inhibit tumor growth/proliferation in vivo

PD-1 mutant 463 inhibited human WT PD-1 binding to PD-L1 (Fig. S7 in Appendix A), PD-L2 (Fig. S8 in Appendix A), or CD80 (Fig. S9 in Appendix A), and therefore reversed the cytokine release

Table 3
Biacore analysis of the selected five PD-1 mutants to bind to PD-L1 and PD-L2.

Mutant	Sample No.	K_a ((mol·L^{-1}·s)$^{-1}$)	K_d (s^{-1})	K_D (mol·L^{-1})
408	PD-L1	9.84×10^{7}	0.572	5.81×10^{-9}
410	PD-L1	1.08×10^{5}	0.137	1.28×10^{-6}
446	PD-L1	5.05×10^{6}	0.178	3.53×10^{-8}
463	PD-L1	9.99×10^{5}	2.060×10^{-3}	2.06×10^{-9}
506	PD-L1	4.25×10^{9}	23.600	5.54×10^{-9}
408	PD-L2	3.40×10^{6}	9.070×10^{-2}	2.67×10^{-8}
410	PD-L2	3.47×10^{10}	4.240×10^{2}	1.22×10^{-8}
446	PD-L2	2.31×10^{6}	2.070×10^{-2}	8.96×10^{-9}
463	PD-L2	2.80×10^{6}	1.950×10^{-2}	6.95×10^{-9}
506	PD-L2	7.70×10^{6}	0.128	1.66×10^{-8}

K_a: association rate constant; K_d: disassociation rate constant; K_D: the equilibrium disassociation constant; $K_D = K_d/K_a$.

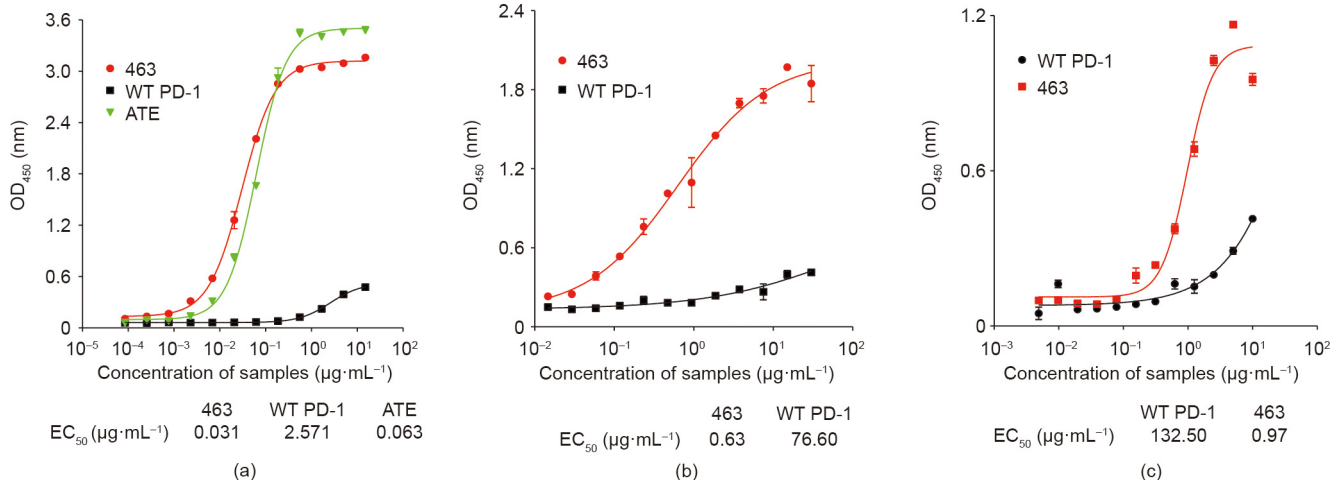

Fig. 3. The PD-1 mutant 463 bound to mouse/human PD-L1 or human PD-L2 in a dose-dependent manner. (a) 463 bound to human PD-L1 in a dose-dependent manner. ATE and WT PD-1 were set as positive controls. The EC_{50} values were 0.031 μg·mL^{-1} (463), 2.571 μg·mL^{-1} (WT PD-1), and 0.063 μg·mL^{-1} (ATE), respectively, suggesting the potential advantage of 463 being able to reverse the PD-1/PD-L1 inhibition. (b) 463 bound to human PD-L2 in a dose-dependent manner. WT PD-1 was set as a positive control. The EC_{50} value of the 463-treated samples was 0.63 μg·mL^{-1}, while the EC_{50} value of the PD-1 group was not reached at a concentration of 100 μg·mL^{-1}, indicating the possibility that 463 could reverse PD-1/PD-L2 inhibition. (c) 463 bound to murine PD-L1 in a dose-dependent manner. WT PD-1 was set as a positive control. The EC_{50} values were 0.97 μg·mL^{-1} (463) and 132.50 μg·mL^{-1} (WT PD-1), respectively; OD_{450}: optical density at 450 nm.

(e.g., IFN-γ) in T cells triggered by the CD3/CD28 pathway in a dose-dependent manner. PD-L1 inhibited T cell activation; however, the anti-PD-1 antibody Opdivo reversed this inhibition. 463 seemed similar to Opdivo but much better than WT PD-1, as the latter showed a weak or no recovery effect (Fig. 4(a)).

In an *in vivo* MC38 xenograft mice model (n = 5 in each group), 463 inhibited tumor growth in a dose-dependent manner, which was similar to the action of ATE in the same dose (10 mg·kg^{-1}). In the group treated with 10 mg·kg^{-1} of 463, the average tumor volume was about 600 mm^3, while in the group treated with WT PD-1, the volume was nearly 2000 mm^3, which was similar to that in the isotype control group (the MIL50 group). More interestingly, even 2 mg·kg^{-1} of 463 possessed better anti-tumor capacity than 10 mg·kg^{-1} of WT PD-1, and resulted in a mean tumor volume of about 1100 mm^3 (10 mg·kg^{-1} 463 vs 10 mg·kg^{-1} WT PD-1, p < 0.05). On day 20, the mice were sacrificed and the tumors were separated and weighed. It was found that 10 mg·kg^{-1} of 463 or even 2 mg·kg^{-1} of 463 showed good anti-tumor effect, as the tumor weights were about (0.6 ± 0.31) and (1.06 ± 0.45) g. Compared with WT PD-1, 10 mg·kg^{-1} 463 was better than 10 mg·kg^{-1} WT PD-1 (1.53 ± 0.81) g at the same dose (Figs. 4(b)–(d), p < 0.05).

4. Discussion

The immune checkpoint molecule PD-1 is a type I transmembrane receptor that exists on the T cell surface and modulates T cell activation. Activated T cells secrete an excess of inflammatory cytokines; however, as a checkpoint molecule for T cell overactivation, PD-1 can bind to its ligands PD-L1 and PD-L2 to limit T cell activity. In cancer environments, PD-L1 molecules are usually overexpressed on the surface of cancer cells; thus, the PD-1/PD-L1 signal enables cancer progression by dampening T cells' anti-tumor immune response [28]. Blockade of the signaling axis between PD-1 and PD-L1 its anti-PD-1 or anti-PD-L1 antibodies has shown remarkable therapeutic success in cancer patients, with objective tumor responses having been observed in clinical trials in melanoma, NSCLC, and other solid tumors [29]. In a phase I clinical trial of patients with metastatic urothelial bladder cancer, the effect was so impressive that tumor shrinkage was observed in 43% of patients; thus, the US Food and Drug Administration granted a breakthrough designation for the tested antibody [30,31]. Globally, anti-PD-1/PD-L1 therapeutic antibody drugs are expanding their indications for cancer treatment. However, anti-PD-1 and anti-PD-L1 antibody treatment is actually still at the

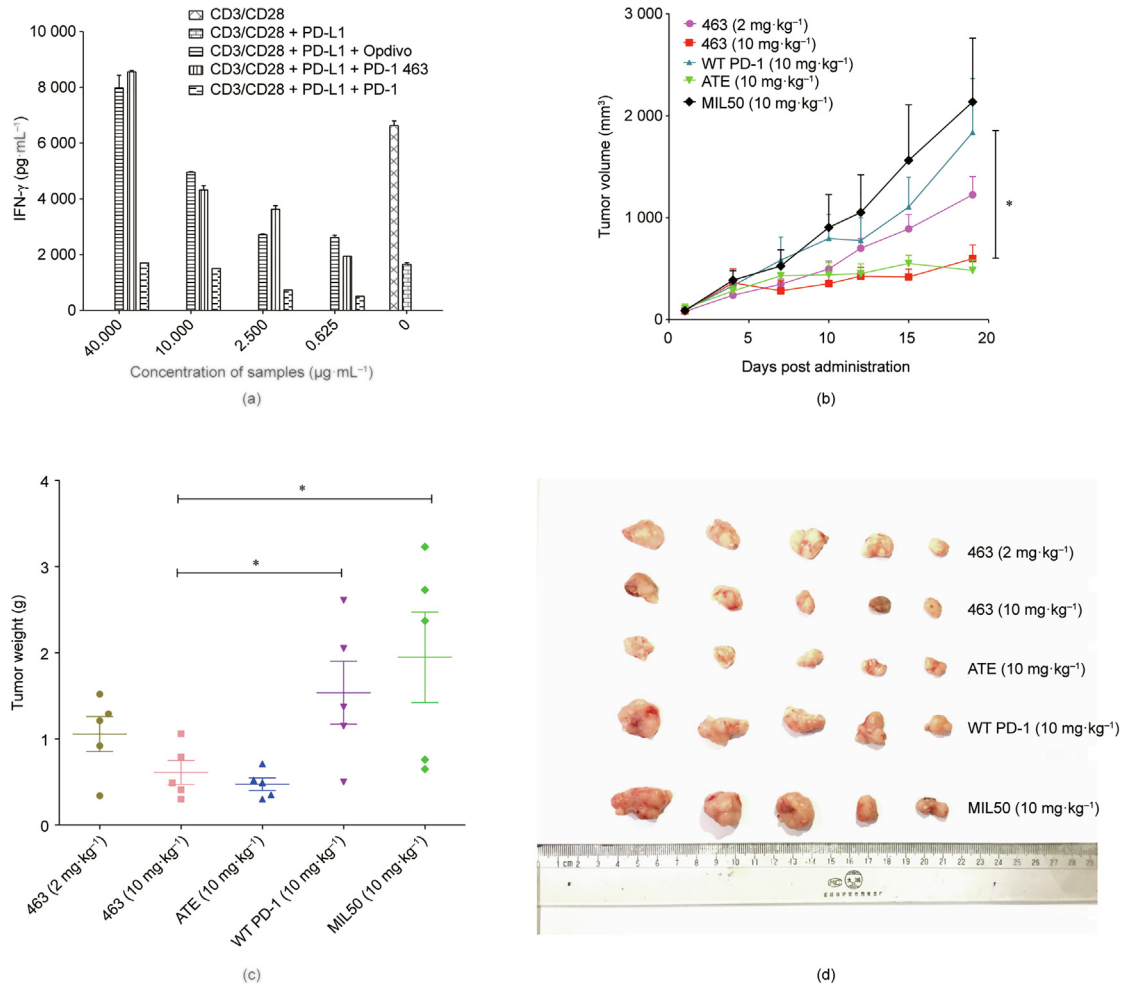

Fig. 4. The biofunction of decoy PD-1 mutant 463 both *in vitro* and *in vivo*. (a) 463 recovered the cytokine release of IFN-γ in T cells triggered by the CD3/CD28 pathway in a dose-dependent manner. Opdivo and PD-1 were set as the controls. 463 showed a similar function to Opdivo. 463 inhibited the growth of tumors in a xenograft mice model: (b) tumor volume of xenograft mice; (c) tumor weight; and (d) tumor stripped from the mice. ATE and PD-1 were set as the positive controls, and the anti-ricin antibody MIL50 was set as the isotype control. 10 mg·kg^{-1} of 463 showed similar anti-tumor activity *in vivo* to 10 mg·kg^{-1} at ezolizumab; however, 10 mg·kg^{-1} WT PD-1 showed very weak function. More interestingly, 2 mg·kg^{-1} of 463 showed better inhibitory activity than WT PD-1. *p < 0.05.

early stage of clinical development, and more checkpoint antibodies and antibody-like proteins are expected to possess enhanced function in pre-clinical or clinical trials. As antibodies have inherent limitations, including poor tumor/tissue penetrance and detrimental Fc-effector functions that deplete immune cells, PD-1/PD-L1-directed immunotherapy could be improved with smaller protein (e.g., decoy PD-1) therapeutics. the high-affinity decoy PD-1 mutant presented herein has the potential to spread more extensively throughout the tumor, whereas anti-PD-L1 antibodies have been found to mostly remain close to the blood vessels and/or at the tumor periphery. Moreover, the high-affinity decoy PD-1 mutant was found to be more effective in treating larger tumors than the PD-L1 antibodies, probably because the high-affinity decoy PD-1 mutant fused to Fc that have a molecular weight halved can enter tumors more effectively [32].

In fact, the crystal structure of murine PD-1 in complex with human PD-L1 [33] or murine PD-L2 [34,35] was reported very early, and the X-ray crystal structure of the human PD-1 complex that forms during its binding to human PD-L1 has been published (PDB: 3RRQ). Well, considering WT PD-1 ectodomain binds to PD-L1 with an affinity of 1×10^6, which is too low to compete with PD-1/PD-L1 complex formation. In order to find a higher affinity decoy PD-1 mutant, we first constructed and theoretically optimized a model of the human PD-1/PD-L1 complex (in solvent, flexible structure) based on previous reported structure. It has been shown that human PD-1/human PD-L1 is associated with significant plasticity within the receptor PD-1, and the PD-L1 are likely to be targeted by small molecules to inhibit the PD-1/PD-L1 axis [36]. According to our model, the key residues were predicted and the alanine scanning experiment further revised the theoretical prediction structure. Further, based on the key residues of PD-1 that bind to PD-L1, we designed and established an epitope-specific cell-surface display library containing millions of PD-1 mutants, from which the higher affinity PD-1 mutant 463 was screened out and shown to have better function than WT PD-1.

Tumor-associated PD-L1 expression predicts the clinical effects of PD-1 immunotherapy; however, PD-L1-negative patients also responded to anti-PD-1 checkpoint treatment, which suggests the existence of other PD-1-associated ligands or pathways. PD-L2 is another known PD-1 ligand, and PD-L2 expression in tumor tissues showed a clear relationship with clinical response in patients with recurrent or metastatic head and neck squamous cell carcinoma (HNSCC) treated with pembrolizumab. PD-L2 distribution was found to be significantly correlated with PD-L1, while PD-L2 expression was detected in certain tumors lacking PD-L1. Both PD-L1 and PD-L2 can predict the therapeutic response of pembrolizumab. Patients with positive PD-L1 and PD-L2 had better treatment response than patients who were only PD-L1 positive. PD-L2 is also an independent predictor of pembrolizumab treatment for progression-free survival (PFS). Compared with PD-L2-negative patients, PD-L2-positive patients had no progression and a longer OS.

To summarize, for both PD-L1- and PD-L2-positive cancer, drugs targeting both PD-1 ligands might have better clinical benefit than drugs targeting only PD-L1 [37]. This study demonstrated that the affinity-matured PD-1 mutant 463 can bind to both PD-L1 and PD-L2 with high affinity (Fig. 3). And unlike the aforementioned PD-1 antibody or PD-L1 antibody, the high-affinity decoy molecule 463 seems to block the three signaling pathways PD-1/PD-L1 (Fig. S7), PD-1/PD-L2 (Fig. S8) and PD-L1/CD80 (Fig. S9). This further clarifies the theoretical basis of 463 as an anti-tumor candidate molecule. Furthermore, 463 reversed the T cell inhibition and stimulated cytokine release (e.g., IFN-γ) triggered by the CD3/CD28 pathway. In an *in vivo* xenograft mice model, 463 inhibited tumor growth with a function similar to that of ATE and was superior to wild type PD-1 (Fig. 4). Our data demonstrates the anti-tumor function of the decoy PD-1 mutant 463 and suggests that it holds potential for PD-1-associated cancer treatment, especially in both PD-L1 and PD-L2 positive cancers.

Acknowledgment

This work was supported by grants from the National Natural Science Foundation of China (21976210).

Compliance with ethics guidelines

Hao Liu, Chunxia Qiao, Naijing Hu, Zhihong Wang, Jing Wang, Jiannan Feng, Beifen Shen, Yuanfang Ma, and Longlong Luo declare that they have no conflict of interest or financial conflicts to disclose.

Appendix A. Supplementary data

Supplementary data to this article can be found online at https://doi.org/10.1016/j.eng.2020.11.011.

References

[1] Pardoll DM. The blockade of immune checkpoints in cancer immunotherapy. Nat Rev Cancer 2012;12(4):252–64.
[2] Blankenstein T, Coulie PG, Gilboa E, Jaffee EM. The determinants of tumour immunogenicity. Nat Rev Cancer 2012;12(4):307–13.
[3] Klump KE, McGinnis JF. The role of reactive oxygen species in ocular malignancy. Adv Exp Med Biol 2014;801:655–9.
[4] Iwai Y, Ishida M, Tanaka Y, Okazaki T, Honjo T, Minato N. Involvement of PD-L1 on tumor cells in the escape from host immune system and tumor immunotherapy by PD-L1 blockade. Proc Natl Acad Sci USA 2002;99(19):12293–7.
[5] Riella LV, Paterson AM, Sharpe AH, Chandraker A. Role of the PD-1 pathway in the immune response. Am J Transplant 2012;12(10):2575–87.
[6] Francisco LM, Sage PT, Sharpe AH. The PD-1 pathway in tolerance and autoimmunity. Immunol Rev 2010;236(1):219–42.
[7] Hawkes EA, Grigg A, Chong G. Programmed cell death-1 inhibition in lymphoma. Lancet Oncol 2015;16(5):e234–45.
[8] Ahmadzadeh M, Johnson LA, Heemskerk B, Wunderlich JR, Dudley ME, White DE, et al. Tumor antigen-specific CD8 T cells infiltrating the tumor express high levels of PD-1 and are functionally impaired. Blood 2009;114(8):1537–44.
[9] Muenst S, Soysal SD, Gao F, Obermann EC, Oertli D, Gillanders WE. The presence of programmed death 1 (PD-1)-positive tumor-infiltrating lymphocytes is associated with poor prognosis in human breast cancer. Breast Cancer Res Treat 2013;139(3):667–76.
[10] Matsuzaki M, Nomizu T, Katagata N, Sakuma T, Momma T, Tachibana K, et al. A case of primary malignant lymphoma of the breast with an unusual ultrasound image. Fukushima J Med Sci 2010;56(2):145–50.
[11] Chemnitz JM, Parry RV, Nichols KE, June CH, Riley JL. SHP-1 and SHP-2 associate with immunoreceptor tyrosine-based switch motif of programmed death 1 upon primary human T cell stimulation, but only receptor ligation prevents T cell activation. J Immunol 2004;173(2):945–54.
[12] Winograd R, Byrne KT, Evans RA, Odorizzi PM, Meyer ARL, Bajor DL, et al. Induction of T-cell immunity overcomes complete resistance to PD-1 and CTLA-4 blockade and improves survival in pancreatic carcinoma. Cancer Immunol Res 2015;3(4):399–411.
[13] Brahmer JR, Tykodi SS, Chow LQ, Hwu WJ, Topalian SL, Hwu P, et al. Safety and activity of anti-PD-L1 antibody in patients with advanced cancer. N Engl J Med 2012;366(26):2455–65.
[14] Hamid O, Robert C, Daud A, Hodi FS, Hwu WJ, Kefford R, et al. Safety and tumor responses with lambrolizumab (anti-PD-1) in melanoma. N Engl J Med 2013;369(2):134–44.
[15] Topalian SL, Hodi FS, Brahmer JR, Gettinger SN, Smith DC, McDermott DF, et al. Safety, activity, and immune correlates of anti-PD-1 antibody in cancer. N Engl J Med 2012;366(26):2443–54.
[16] Motzer RJ, Rini BI, McDermott DF, Redman BG, Kuzel TM, Harrison MR, et al. Nivolumab for metastatic renal cell carcinoma: results of a randomized phase II. trail. J Clin Oncol 2015;33(13):1430–7.
[17] Rizvi NA, Mazières J, Planchard D, Stinchcombe TE, Dy GK, Antonia SJ, et al. Activity and safety of nivolumab, an anti-PD-1 immune checkpoint inhibitor, for patients with advanced, refractory squamous non-small-cell lung cancer (CheckMate 063): a phase 2, single-arm trial. Lancet Oncol 2015;16(3):257–65.

[18] Topalian SL, Drake CG, Pardoll DM. Immune checkpoint blockade: a common denominator approach to cancer therapy. Cancer Cell 2015;27(4):450–61.
[19] Dömling A, Holak TA. Programmed death-1: therapeutic success after more than 100 years of cancer immunotherapy. Angew Chem Int Ed Engl 2014;53(9):2286–8.
[20] Homet Moreno B, Ribas A. Anti-programmed cell death protein-1/ligand-1 therapy in different cancers. Br J Cancer 2015;112(9):1421–7.
[21] Mahoney KM, Freeman GJ, McDermott DF. The next immune-checkpoint inhibitors: PD-1/PD-L1 blockade in melanoma. Clin Ther 2015;37(4):764–82.
[22] Chen DS, Mellman I. Oncology meets immunology: the cancer-immunity cycle. Immunity 2013;39(1):1–10.
[23] Scott AM, Wolchok JD, Old LJ. Antibody therapy of cancer. Nat Rev Cancer 2012;12(4):278–87.
[24] Sznol M, Chen L. Antagonist antibodies to PD-1 and B7–H1 (PD-L1) in the treatment of advanced human cancer. Clin Cancer Res 2013;19(5):1021–34.
[25] Lipson EJ, Forde PM, Hammers HJ, Emens LA, Taube JM, Topalian SL. Antagonists of PD-1 and PD-L1 in cancer treatment. Semin Oncol 2015;42(4):587–600.
[26] Cheng X, Veverka V, Radhakrishnan A, Waters LC, Muskett FW, Morgan SH, et al. Structure and interactions of the human programmed cell death 1 receptor. J Biol Chem 2013;288(17):11771–85.
[27] Luo L, Wang S, Lang X, Zhou T, Geng J, Li X, et al. Selection and characterization of the novel anti-human PD-1 FV78 antibody from a targeted epitope mammalian cell-displayed antibody library. Cell Mol Immunol 2018;15(2):146–57.
[28] Sakuishi K, Apetoh L, Sullivan JM, Blazar BR, Kuchroo VK, Anderson AC. Targeting Tim-3 and PD-1 pathways to reverse T cell exhaustion and restore anti-tumor immunity. J Exp Med 2011;208(6):1331.
[29] Brahmer JR. PD-1-targeted immunotherapy: recent clinical findings. Clin Adv Hematol Oncol 2012;10(10):674–5.
[30] Choueiri TK, Figueroa DJ, Fay AP, Signoretti S, Liu Y, Gagnon R, et al. Correlation of PD-L1 tumor expression and treatment outcomes in patients with renal cell carcinoma receiving sunitinib or pazopanib: results from COMPARZ, a randomized controlled trial. Clin Cancer Res 2015;21(5):1071–7.
[31] Powles T, Eder JP, Fine GD, Braiteh FS, Loriot Y, Cruz C, et al. MPDL3280A (anti-PD-L1) treatment leads to clinical activity in metastatic bladder cancer. Nature 2014;515(7528):558–62.
[32] High-affinity PD-1 protein has potential. Cancer Discov 2015;5(11):1115–6.
[33] Lin DY, Tanaka Y, Iwasaki M, Gittis AG, Su HP, Mikami B, et al. The PD-1/PD-L1 complex resembles the antigen-binding Fv domains of antibodies and T cell receptors. Proc Natl Acad Sci USA 2008;105(8):3011–6.
[34] Freeman GJ. Structures of PD-1 with its ligands: sideways and dancing cheek to cheek. Proc Natl Acad Sci USA 2008;105(30):10275–6.
[35] Lázár-Molnár E, Yan Q, Cao E, Ramagopal U, Nathenson SG, Almo SC. Crystal structure of the complex between programmed death-1 (PD-1) and its ligand PD-L2. Proc Natl Acad Sci USA 2008;105(30):10483–8.
[36] Zak KM, Kitel R, Przetocka S, Golik P, Guzik K, Musielak B, et al. Structure of the complex of human programmed death 1, PD-1, and its ligand PD-L1. Structure 2015;23(12):2341–8.
[37] Yearley JH, Gibson C, Yu N, Moon C, Murphy E, Juco J, et al. PD-L2 expression in human tumors: relevance to anti-PD-1 therapy in cancer. Clin Cancer Res 2017;23(12):3158–67.